RESEARCH ARTICLE

NANO · MICRO small
www.small-journal.com

Twisting-Induced Phonon Localization and Ultralow Thermal Conductivity in Penta-$PdTe_2$ Bilayer Revealed by a Universal Machine-Learning Potential

Chenxin Zhang, Qian Wang, and Puru Jena*

The recent synthesis of penta-$PdTe_2$ sheet highlights the growing interest in pentagonal topologies for developing new 2D materials. Distinct from previously synthesized 2D pentagonal materials, penta-$PdTe_2$ possesses the heaviest elemental composition to date, rendering its phonon transport properties particularly intriguing. In this study, the universal machine-learning potential, NEP89, is fine-tuned using high-accuracy first-principles data spanning monolayer, bilayer, and twisted configurations of penta-$PdTe_2$ and achieving an energy prediction error within 2.3 meV atom^{-1}. Leveraging the homogeneous non-equilibrium molecular dynamics simulations with the fine-tuned machine-learning potential and Wigner transport theory, the phonon transport behavior and lattice thermal conductivity is systematically investigated. These results reveal that interlayer stacking reduces the bilayer thermal conductivity to 28.00% of the monolayer value, while interlayer twisting induces a further reduction to 76.19%, leading to an ultralow thermal conductivity of (0.30 ± 0.059) W m^{-1} K^{-1}. These findings demonstrate that the interplay of pentagonal topology, strategic elemental composition, and twist engineering provides an effective route for tuning phonon transport in 2D materials.

1. Introduction

Modulating the functionalities of 2D materials has attracted considerable research interest in recent years. Beyond conventional strategies such as doping, defect engineering, and the application of external fields, interlayer twisting has emerged as a reversible, non-destructive, and continuously tunable approach to tailoring material properties without altering chemical composition.[1,2] By rotating one atomic layer relative to another, a lattice misalignment is introduced, giving rise to moiré patterns that break translational symmetry and modify interlayer coupling. This structural modulation can induce substantial changes in electronic properties and significantly influence phonon transport both within and between layers by altering phonon-phonon and phonon-interface scattering rates. Consequently, interlayer twisting offers a precise method for tuning lattice thermal conductivity with the twist-angle acting as a critical control parameter.[3–6]

Among various 2D systems, pentagon-based 2D materials (penta-sheets) are particularly interesting due to their intrinsic lattice strain and reduced symmetry,[7] which strongly influence phonon lifetimes and the anisotropy of heat transport.[8] These characteristics usually lead to low lattice thermal conductivity, making penta-sheets ideal candidates for exploring phonon dynamics and thermal transport properties. Very recently, penta-$PdTe_2$ was successfully synthesized,[9] representing the heaviest experimentally realized member of the penta-material family. Its combination of large atomic mass and complex pentagonal lattice geometry makes it especially well-suited for investigating phonon-mediated heat conduction and exploring how thermal transport responds to interlayer twisting.

Previous theoretical studies on penta-$PdTe_2$ have primarily focused on its catalytic,[10] optical,[11,12] and magnetic[11] properties. Although Lan[13] and Li et al.[14] explored its thermal transport properties using the Boltzmann transport equation (BTE)[15] and three-phonon theory,[16] their reported lattice thermal conductivity values vary widely, ranging from 0.41 to 5.90 W m^{-1} K^{-1}, reflecting substantial uncertainty stemming from the limited accuracy of computational methods available at the time. More recent advances suggest that four-phonon scattering processes[17] and phonon coherence effects[18,19] play important roles in the thermal transport of pentagonal materials,[3,5,6,8] emphasizing the necessity of including higher-order phonon interactions when calculating the thermal conductivity of strongly anharmonic 2D materials.

In our previous studies, machine-learning interatomic potentials such as the moment tensor potential (MTP)[20] and Neuroevolution potential (NEP),[21,22] have demonstrated strong capability in describing phonon properties of penta-sheets.[5,6] Building on the NEP framework, a universal machine-learning

C. Zhang, Q. Wang
School of Materials Science and Engineering
Peking University
Beijing 100871, China
E-mail: qianwang2@pku.edu.cn
P. Jena
Department of Physics
Virginia Commonwealth University
Richmond, VA 23284, USA

The ORCID identification number(s) for the author(s) of this article can be found under https://doi.org/10.1002/smll.202509794

DOI: 10.1002/smll.202509794

potential, NEP89,[23] was recently developed to achieve both high accuracy and excellent transferability across diverse atomic configurations. By incorporating the atom-centered descriptors constructed with Chebyshev and Legendre polynomials, NEP89 enables reliable predictions of energies and forces. Its universal and flexible architecture allows it to be fine-tuned for accurately describing the complex atomic interactions presented in twisted penta-$PdTe_2$, while remaining relatively low computational cost.

In this study, we construct the geometric structure of monolayer penta-$PdTe_2$ based on experimental data,[9] and generate its bilayer and twisted configurations by stacking and matching the common lattice vectors.[24] To accurately capture interatomic interactions, a high-accuracy dataset from first-principles calculations is employed to fine-tune the NEP89 potential. By integrating the refined NEP89 with the homogeneous non-equilibrium molecular dynamics method,[25,26] we calculate the lattice thermal conductivity of the monolayer, bilayer, and twisted structures of penta-$PdTe_2$. This investigation addresses two key questions: 1) Can the thermal conductivity of pentagonal 2D materials be reduced to an ultralow value below 0.5 W m^{-1} K^{-1}, and 2) how does twisting influence phonon transport in penta-$PdTe_2$ bilayers?

2. Computational Methods

Calculations based on density functional theory (DFT) are performed using the projector-augmented wave method (PAW)[27,28] implemented in the Vienna ab initio simulation package (VASP).[29] The electronic exchange-correlation interaction for electrons is treated by using the Perdew-Burke-Ernzerhof functional (PBE)[30] within the generalized gradient approximation (GGA).[31] To account for the van der Waals (vdW) interaction, the optB88 method[32] is employed. A kinetic energy cutoff of 500 eV is used for the wave function basis set. Ab initio molecular dynamics (AIMD) simulations are carried out for the monolayer, bilayer, and twisted penta-$PdTe_2$ sheets at temperatures ranging from 200 to 700 K for generating diverse atomic configurations for training the NEP89 model (see details of the test set in Figure S1, Supporting Information).[23]

Based on the DFT calculations using a $3 \times 3 \times 1$ **k**-point grid to obtain energy and interatomic force information, we use 140 structures as the extracted input configurations for fine-tuning the dataset of NEP89.[23] The training is performed over 5×10^5 steps as the default settings.

The homogeneous non-equilibrium molecular dynamics (HNEMD) simulations (details can be found in Figure S2, Supporting Information) are carried out employing the fine-tuned potential NEP89[23] and using the GPUMD package.[25,26] To minimize the influence of finite-size effects in the molecular dynamics (MD) simulations, we use supercells of $15 \times 15 \times 1$ for both the monolayer and bilayer penta-$PdTe_2$ structures, and $6 \times 6 \times 1$, $4 \times 4 \times 1$ and $4 \times 4 \times 1$ for the twisted structures with twist angles of 36.87°, 22.62° and 41.13°, respectively. The structures are fully relaxed for 1 ns, and then 10 independent HNEMD simulations are performed for the same initial configuration with different random seeds in the NVT ensemble at 300 K with a timestep of 1 fs for 10 ns. To ensure the reliability of simulations, we perform an energy minimization by applying the fast inertial relaxation engine (FIRE) method[33] implemented in the GPUMD package. The force convergence criterion of FIRE minimization is set to 3×10^{-5} eV $Å^{-1}$.

According to the Winger framework of lattice thermal transport,[18,19] the total lattice thermal conductivity (κ_L) is divided into the particle-like contribution (κ_L^P) and the coherence contribution (κ_L^C):

$$\kappa_L = \kappa_L^P + \kappa_L^C \tag{1}$$

The microscopic description of κ_L^P is derived from the phonon Boltzmann transport equation[15] within the framework of phonon scattering. The intrinsic κ_L^P can be expressed as follows:

$$\kappa_L^{P,\alpha\beta} = \frac{1}{k_B T^2 \Omega N} \sum_{\mathbf{q}} \sum_i \bar{N}_{\mathbf{q}i}(\bar{N}_{\mathbf{q}i}+1)(\hbar\omega_{\mathbf{q}i})^2 V_{\mathbf{q}i}^{\alpha} V_{\mathbf{q}i}^{\beta} \tau_{\mathbf{q}i} \tag{2}$$

Where α and β are the directions of the Cartesian coordinate system, $\hbar$, k_B, T, N, and Ω are the reduced Planck constant, Boltzmann constant, temperature, number of phonon wave vectors, and lattice volume, respectively. $\omega_{\mathbf{q}i}$ and $\bar{N}_{\mathbf{q}i}$ are the angular frequencies and the equilibrium Bose-Einstein distribution, indexed by wave vector **q** with the branch i, respectively. $V_{\mathbf{q}i}$ is the phonon group velocity, and $\tau_{\mathbf{q}i} = 1/\Gamma_{\mathbf{q}i}$ is the phonon lifetime, where $\Gamma_{\mathbf{q}i}$ is the phonon linewidth (scattering rate) of each phonon.

In addition, κ_L^C is calculated by using the following Equation (3)[18,19]:

$$\kappa_L^{C,\alpha\beta} = \frac{\hbar^2}{k_B T^2 \Omega N} \sum_{\mathbf{q}} \sum_{i \neq j} \frac{\omega_{\mathbf{q}i}+\omega_{\mathbf{q}j}}{2} V_{\mathbf{q}i}^{\alpha} V_{\mathbf{q}j}^{\beta} \times \frac{\omega_{\mathbf{q}i}\bar{N}_{\mathbf{q}i}(\bar{N}_{\mathbf{q}i}+1)+\omega_{\mathbf{q}j}\bar{N}_{\mathbf{q}j}(\bar{N}_{\mathbf{q}j}+1)}{4(\omega_{\mathbf{q}i}-\omega_{\mathbf{q}j})^2+(\Gamma_{\mathbf{q}i}+\Gamma_{\mathbf{q}j})^2} \times (\Gamma_{\mathbf{q}i}+\Gamma_{\mathbf{q}j}) \tag{3}$$

Where $V_{\mathbf{q}ij}$ represents the generalized velocity matrix along different directions. The phonon linewidths required by the Wigner transport equation (WTE) calculations are obtained with the spectral energy density (SED) method[34] implemented in the Dynaphopy package through the Fourier transform.[34,35] The MD trajectories used for the SED and phonon lifetime calculations are set to 5×10^5 steps with a time step of 1 fs, corresponding to a total trajectory length of 0.5 ns. The **q**-mesh grids are set as $12 \times 12 \times 1$ for the monolayer and bilayer, $6 \times 6 \times 1$ for the 36.87° twisted structure, and $4 \times 4 \times 1$ for the 22.62° and 41.13° twisted structures. The input MD trajectories are calculated by the LAMMPS package[36] using the NVT ensemble. For the WTE calculations, the supercell thickness is defined as the maximum interatomic distance along the z-direction of the structure plus twice the van der Waals radius of the Te atoms.[5,37]

3. Results and Discussion

3.1. Geometric Structures

We built the penta-$PdTe_2$ monolayer and bilayer structures using the lattice parameters from experimental studies on penta-sheets.[9,38] To get well stacked twisted structures, we used the

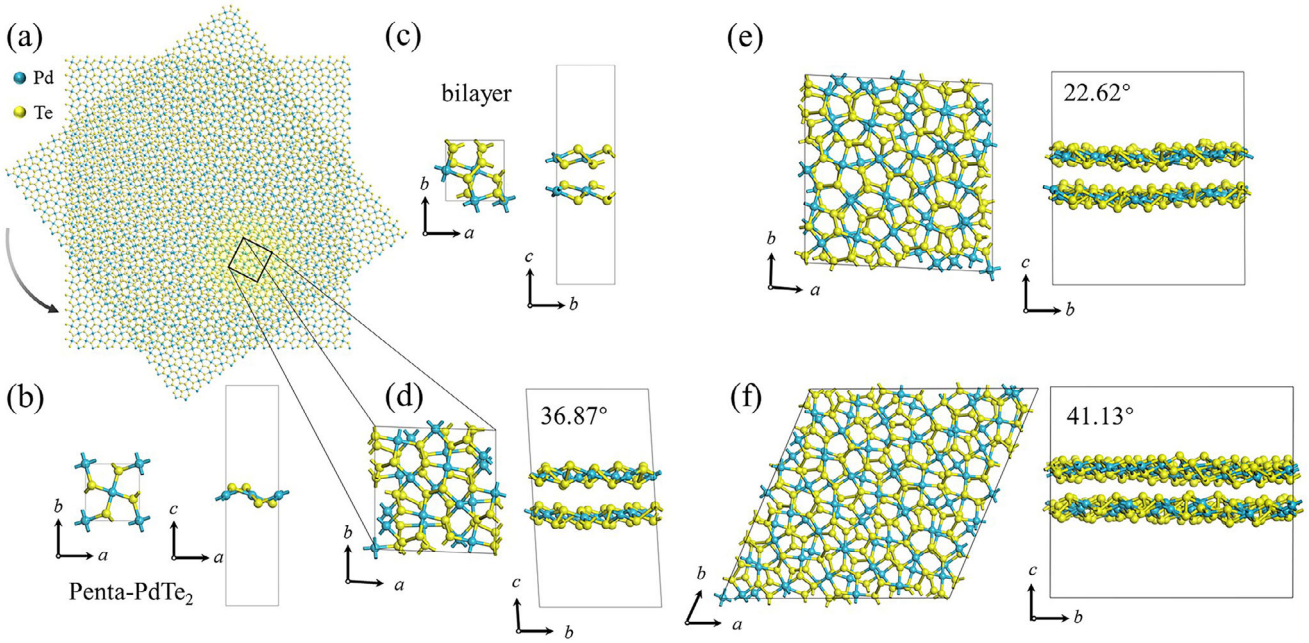

Figure 1. a) Schematic diagram of the interlayer twist in penta-$PdTe_2$ bilayer. b–f) Top and side views of the unit cells of the monolayer, bilayer, and twisted penta-$PdTe_2$ structures with angles of 36.87°, 22.62°, and 41.13°, respectively.

CellMatch package[24] to generate more than 100 twisted structures for bilayer penta-$PdTe_2$ by matching the common lattice vectors, and selected three structures with twist angles of 36.87°, 22.62° and 41.13° for further study because they contain smaller number of atoms in their unit cells (60, 156 and 276 atoms, respectively) with higher symmetry as compared with the other twisted structures. The schematic diagram and optimized atomic configurations of the monolayer, bilayer, and the selected three structures are presented in **Figure 1**. The detailed lattice parameters of the five systems are given in Table S1 (Supporting Information). The monolayer penta-$PdTe_2$ possesses $P2_1/c$ (No. 14) symmetry, and the untwisted pristine bilayer sheet has a $Pca2_1$ (No. 29) symmetry, while the symmetry of the twisted structures is reduced to $P1$ due to the complex stacking configurations.

As shown in Figure 1d–f, the geometric anisotropy observed in the pristine sheet is significantly reduced with increased lattice complexity induced by twisting. The optimized twisted structures exhibit noticeable out-of-plane undulation, reminiscent of that reported in twisted bilayer penta-$PdSe_2$,[6] originating from twisting-induced in-plane stress that would affect the thermal transport properties. We also calculated the electronic band structures of monolayer and bilayer penta-$PdTe_2$. The monolayer is an indirect semiconductor with an energy band gap of 1.28 eV, whereas the bilayer exhibits a significantly reduced gap of 0.63 eV due to the interlayer stacking effect. As plotted in Figure S3 (Supporting Information), the conduction band minimum (CBM) and valence band maximum (VBM) of the monolayer are contributed mainly from the d_{yz} orbital of the Pd atom and the p_x orbital of the Te atom in the unit cell, respectively. On the other hand, for the bilayer structure, the CBM and VBM are primarily contributed by the d_{z^2} orbitals of Pd atoms, respectively, resulting in a reduced band gap.

3.2. Fine-Tuning the Machine Learning Potential NEP89

To accurately simulate the phonon properties of the constructed monolayer, bilayer, and twisted penta-$PdTe_2$ structures while keeping the computational cost within a reasonable range, we employed the recently developed machine-learning potential NEP89, which is designed for high accuracy and broad transferability across diverse atomic structures. It employs atom decomposed total energy and atom-centered descriptors to achieve smooth and consistent energy-force predictions. With a specialized fine-tuning training process, MD simulation using the NEP89 potential is capable of accurately modeling a broad range of materials and structural configurations. To this end, we performed high-accuracy DFT calculations on perturbed configurations of the monolayer, bilayer, and twisted penta-$PdTe_2$ structures obtained from AIMD trajectories to extract energies and interatomic forces as training data to fine-tune the NEP89 potential. The overall workflow is illustrated in **Figure 2a**. After 5×10^5 training steps, the accuracy of the potential continually improved and eventually converged, as shown in Figure 2b. The energy prediction error (RMSE) decreases from an initial 14.9 to 2.3 meV $atom^{-1}$, ensuring the reliability of subsequent simulations. The phonon spectra of the selected structures calculated by using the fine-tuned potential show no imaginary frequencies (see Figure S4, Supporting Information), further validating both the accuracy of the NEP89 potential and the dynamical stability of the selected systems. Furthermore, we compare the phonon dispersion of monolayer penta-$PdTe_2$ calculated using the trained potential with that obtained from DFT combined with the finite-displacement method (see details in Figure S5, Supporting Information), showing good consistency. According to the semiconducting property of the penta-$PdTe_2$ family, their thermal transport properties are dominated by lattice vibrations. Therefore, we

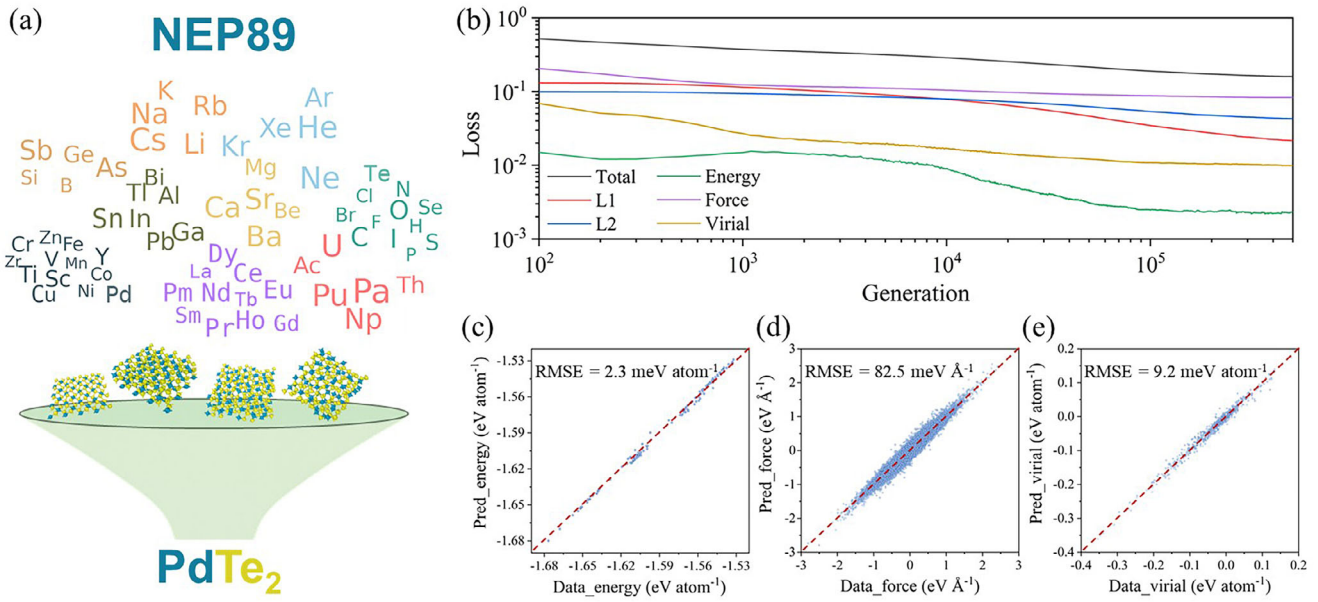

Figure 2. a) Schematic diagram of the fine-tuning process, and b) trained generation of the fine-tuned NEP89. c–e) Comparison of the potential energy, atomic force, and virial components between DFT calculations and NEP89-based predictions of the training datasets with perturbed monolayer, bilayer, and twisted penta-$PdTe_2$ structures.

employed this potential to study the thermal transport properties of penta-$PdTe_2$.

3.3. Lattice Thermal Conductivity

We investigated the thermal transport properties of the selected structures by calculating their lattice thermal conductivity using the HNEMD method implemented in the GPUMD package[25,26] combined with our fine-tuned NEP89 potential at 300 K.[21,22] The results are presented in **Figure 3**a and compared with other synthesized pentagon-based 2D materials.[3,5,6,8,13,39] The κ_L of monolayer penta-$PdTe_2$ along the crystallographic *a*- and *b*-directions are (1.80 ± 0.15) and (4.50 ± 0.34) W m^{-1} K^{-1}, respectively, exhibiting significant anisotropy. Notably, the result for *b*-direction is slightly lower than that of the previous study (5.90 W m^{-1} K^{-1}) by Lan et al.[13] but higher than that of 0.83 W m^{-1} K^{-1} by Li et al.[14] These differences may originate from the limitation of previous studies that only considered three-phonon

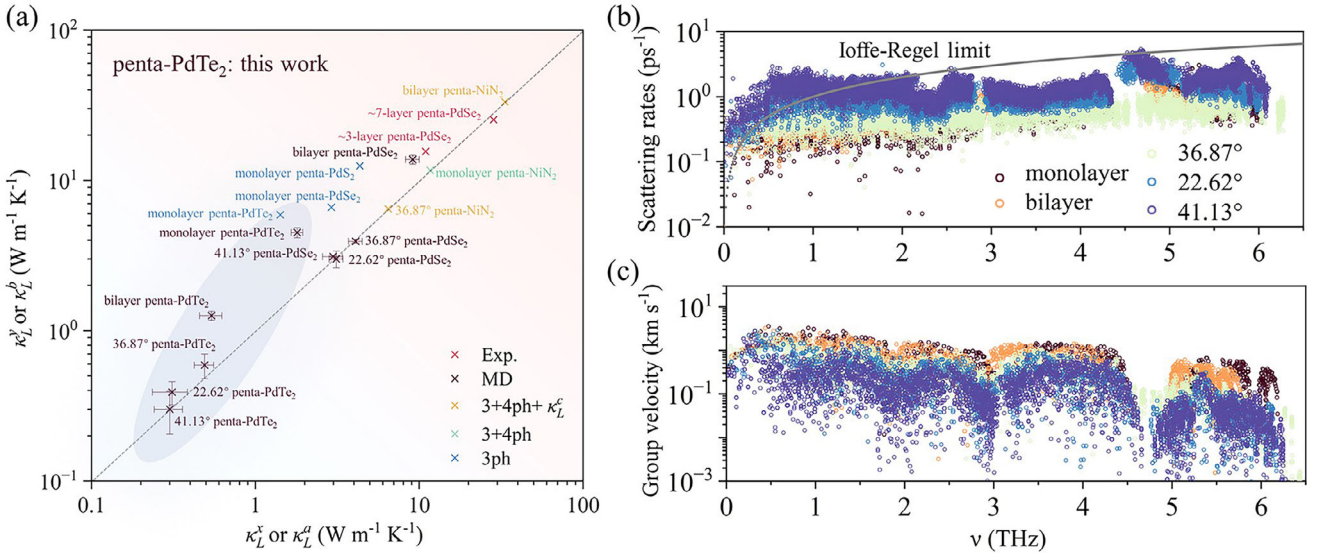

Figure 3. a) Calculated κ_L of the selected penta-$PdTe_2$ structures compared with other synthesized pentagonal 2D materials; methods labeled in the legend are arranged in the order of complexity of the phonon transport mechanisms involved. b) Phonon scattering rates, and c) phonon group velocities of the monolayer, bilayer, and twisted penta-$PdTe_2$.

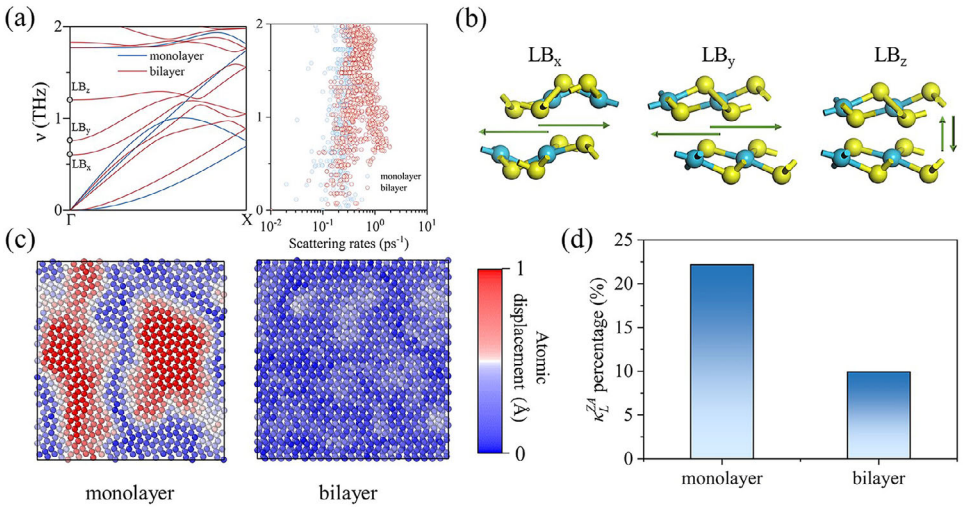

Figure 4. a) LB phonon modes in bilayer penta-$PdTe_2$ as compared with monolayer structure and the phonon scattering rates of the corresponding frequency region, b) geometric illustration of LB modes. c) Comparison between the atomic displacements, and d) the ratio of ZA modes contributing to κ_L of monolayer and bilayer structures.

interactions and employed relatively small supercells. Previous studies have shown that higher-order anharmonicity and finite-temperature renormalization can significantly influence lattice thermal conductivity.[40,41] These effects are fully captured in our calculations by employing the HNEMD method in combination with our fine-tuned NEP89 potential, which naturally incorporates high-order phonon interactions as well as finite-temperature and phonon coherence effects.[6,42] Consequently, the corresponding values for bilayer penta-$PdTe_2$ in the crystallographic directions (*a* and *b*) are calculated to be (0.54 ± 0.084) and (1.26 ± 0.087) W m^{-1} K^{-1}, only ≈7.60% of the $\kappa_L$of bilayer penta-$PdSe_2$,[6] arising mainly due to the heavy mass of Te atom in this penta-sheet, making them the lowest value ever reported among all the synthesized penta-sheets.

Moreover, the introduction of further twisting significantly reduces the thermal conductivity $\kappa_L$compared to the bilayer. For instance, the κ_L of twisted penta-$PdTe_2$ with a twist angle of 36.87° at 300 K is calculated to be (0.49 ± 0.067) and (0.59 ± 0.11) W m^{-1} K^{-1} in the *a*- and *b*-directions, respectively. This shows a decreasing trend as the number of atoms in the unit cells increases. The corresponding values of the 22.62° structure are (0.31 ± 0.075) and (0.39 ± 0.069) W m^{-1} K^{-1}, respectively. While the lowest value appears at a twist angle of 41.13° with the largest unit cell containing 276 atoms, reaching extremely low values of (0.30 ± 0.059) and (0.30 ± 0.095) W m^{-1} K^{-1} in the *a*- and *b*-directions, respectively. This is only 23.80% of that of the bilayer one. In comparison with all the other synthesized 2D pentagonal materials, calculated at different theoretical levels, the lattice thermal conductivity of the twisted penta-$PdTe_2$ structure with 41.13° angle holds a record-low value, as illustrated in Figure 3a.[3,5,6,8,13,39]

As shown in Figure 3b,c, the twisted structures exhibit increased phonon scattering rates and reduced group velocities. The enhanced phonon scattering is caused by the increased anharmonicity and complex atomic neighboring environment induced by twisting. In addition, the Brillouin zone folding and phonon modes repulsion result in the flattening of phonon branches, thereby reducing the group velocity (see Figure S4, Supporting Information). Especially, partial scattering rates of the twisted structures with 22.62° and 41.13° angles exceed the Ioffe-Regel limit,[19,43] exhibiting strong anharmonicity. We also note that twisting weakens the anisotropy of the thermal transport properties of this penta-sheet.

For a better understanding of the results, we further calculated the normalized participation ratio (NPR_q)[44,45] for measuring the degree of phonon localization, defined as:

$$NPR_q = 1/\left[N_a \sum_{i=1}^{N_a} \left(\sum_{\alpha}^{3} \varepsilon_{qi\alpha}^2 \right)^2 \right] \quad (4)$$

Where $\varepsilon_{qi\alpha}$ is the eigenvector of a phonon mode **q**; the lower the NPR_q, the more localized is the phonon. When the value of NPR_q reaches 1.0, all the atoms in the unit cell participate in the specific phonon mode. As illustrated in Figure S6 (Supporting Information), the average NPR_q values of twisted structures are much lower than those of the monolayer and bilayer ones, indicating a substantial enhancement in the localization of phonon modes, due to the enhanced anharmonicity and reduced symmetry.[46] These results are in agreement with previous studies of localized vibrations in layered Si/Ge heterostructures and layered Bi_2Se_3 from both theoretical and experimental perspectives, showing that vibrational localization indeed hinders thermal transport and leads to ultralow thermal conductivity.[47,48]

3.4. Stacking Effect on the Lattice Vibrations of the Bilayer

Interestingly, the thermal conductivity of penta-$PdTe_2$ bilayer is significantly lower than that of the monolayer, with the value along the *b*-direction reduced to only 28.00% of the monolayer value. To uncover the mechanism behind this stacking-induced tuning of lattice thermal conductivity, we analyzed the phonon

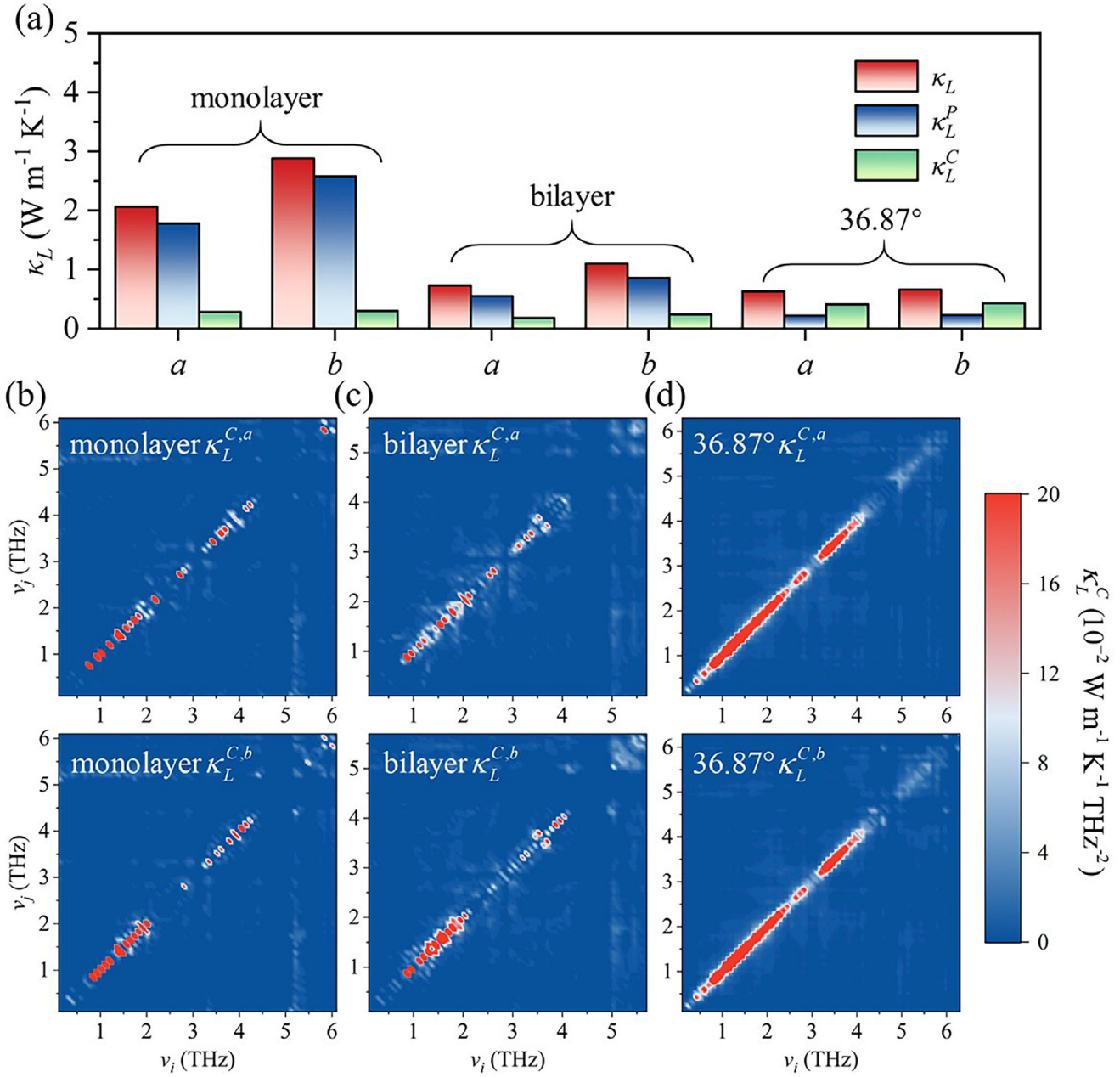

Figure 5. a) Lattice thermal conductivity κ_L in the *a*- and *b*-directions of monolayer, bilayer, and 36.87° twisted penta-$PdTe_2$ calculated by the WTE method. b–d) The contribution of coherent modes to the total coherent thermal conductivity.

scattering rates and the stacking-induced emergent phonon modes in both monolayer and bilayer structures. As shown in **Figure** 4a, the phonon scattering rates of the bilayer structure exhibit a pronounced peak around 1.0 THz compared to those of the monolayer, which corresponds to the emergence of interlayer breathing (LB) modes induced by stacking. The geometric illustrations of the LB modes along the *x*-, *y*-, and *z*-directions (LB_x, LB_y, and LB_z) are shown in Figure 4b. Normally, out-of-plane acoustic (ZA) modes typically contribute significantly to the κ_L of 2D materials. The introduction of LB modes may suppress the contribution of ZA modes to the overall thermal transport. To verify this hypothesis, we analyzed the MD trajectories of monolayer and bilayer penta-$PdTe_2$ near the excitation temperatures of the LB modes (~50 K). As shown in the atomic displacement fields in Figure 4c, atomic vibrations in the bilayer structure are significantly suppressed around 50 K. Furthermore, we quantified the contribution of ZA modes to κ_L and found that it decreases from 21.18% in the monolayer to 9.93% in the bilayer, confirming that the LB modes introduced by stacking effectively suppress the ZA-mode contributions and lead to the reduction in thermal conductivity of the bilayer structure.

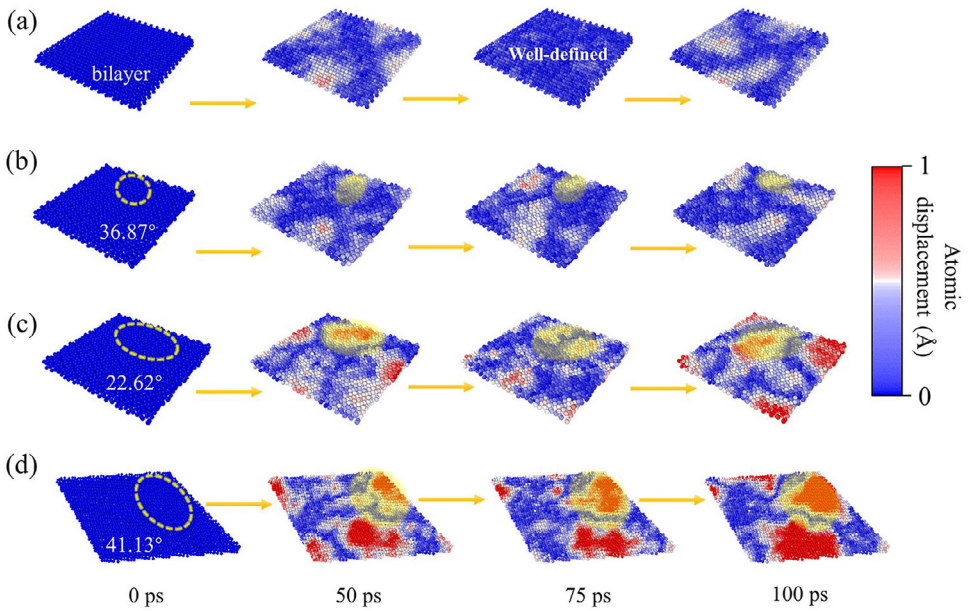

Figure 6. a–d) Atomic displacement trajectories of the bilayer, 36.87°, 22.62°, and 41.13° twisted structures within 100 ps at 300 K. The yellow circles and highlighted regions mark the areas where similar vibrational patterns emerge and move.

3.5. Phonon Coherence Contributions and Localization

To further understand the complex phonon behavior in twisted penta-$PdTe_2$, we employed the WTE method to quantify the respective contributions of particle-like propagation and wave-like transport to the lattice thermal conductivity (κ_L), namely, phonon scattering (κ_L^P) and phonon coherence (κ_L^C). Due to the majority of phonon scattering rates in the 22.62° and 41.13° twisted structures exceeding the Ioffe-Regel limit, beyond the valid regime of the WTE theory, we restrict our discussion here to the monolayer, bilayer, and 36.87° twisted structures. As shown in **Figure 5a**, the WTE results are in good agreement with those obtained from HNEMD simulations. By analyzing the relative contributions of κ_L^P and κ_L^C, one can see that due to the increased structural complexity and anharmonicity induced by twisting, κ_L^C gradually becomes the dominant transport mechanism. In the 36.87° twisted structure, the coherent contribution reaches up to ≈65.15% of the total thermal conductivity. According to Equation (3), further analysis of the two-mode contributions to κ_L^C reveals that as the average phonon frequency interval decreases due to twisting, phonon scattering is enhanced synergistically, and more coupled phonon modes begin to participate in coherent transport, leading to an increase in κ_L^C. As illustrated in Figure 5b–d, more degenerate and non-degenerate phonon modes become involved in coherence.

To elucidate how twisting induces anharmonicity at the atomic scale in penta-$PdTe_2$, we calculated the atomic force distribution after 1 ns of NVT ensemble relaxation. As shown in Figure S7 (Supporting Information), a pronounced enhancement of local atomic forces and a spatially inhomogeneous distribution appear after twisting. The inhomogeneity becomes more significant with increasing structural complexity. This suggests that many atoms deviate from equilibrium positions due to the complex neighboring environment after twisting, hindering the propagation of ideal phonon modes and resulting in strong anharmonicity. In addition, to illustrate the ultralow lattice thermal conductivity of the two twisted structures with 22.62° and 41.13° angles, we provide a real-space representation of phonon coherence and localization in **Figure 6**. In the ensemble-averaged trajectories of 10 MD simulations at 300 K, all atomic displacement fields are calculated by using the initial configuration to provide a reliable analysis of atomic vibrations. We observe that the atomic displacement field in the bilayer structure exhibits similar displacement with periodic patterns, which is strong evidence for the existence of well-defined phonons. In the twisted structure with a twist angle of 36.87°, a slight displacement diffusion phenomenon occurs without significant accumulation. However, the trajectories of 22.62° and 41.13° twisted structures lose the periodic vibration characteristics, exhibiting long-lived displacement patterns. Especially, for the 41.13° structure, as shown in Figure 6d, the strong anharmonicity drives the systems into a liquid-like phonon transport regime.[19] Over an ultralong period of 50 ps, atomic vibrations remain accumulated at the same island-like position, as marked by the highlighted regions, exhibiting distinct localization characteristics. This localized behavior further suppresses thermal energy transport and ultimately leads to the extremely low values of the κ_L.

4. Conclusion

To gain a deeper insight into the properties of the recently synthesized penta-$PdTe_2$, we investigated the phonon transport and lattice thermal conductivity of its bilayer and twisted structures. Calculations are carried out by employing the homogeneous non-equilibrium molecular dynamics method and the fine-tuned universal machine learning potential, NEP89, trained on first-principles data. Owing to its heavy atomic mass and intrinsically buckled geometry, bilayer penta-$PdTe_2$ exhibits the lowest

lattice thermal conductivity among all experimentally synthesized pentagonal 2D materials. Particularly, under interlayer twisting, the interlayer breathing modes suppress the contributions from the out-of-plane acoustic (ZA) phonons, the increased structural complexity induced by twisting simultaneously enhancing its anharmonicity. These effects synergistically drive the thermal conductivity to a record-low value of (0.30 ± 0.059) W m^{-1} K^{-1}. Further analysis based on the Wigner transport equation reveals a twisting-induced transition in phonon transport behavior, from enhanced phonon coherence in the 36.87° configuration as compared to the bilayer form to phonon localization in the 22.62° and 41.13° structures due to the strong anharmonicity, exceeding the Ioffe-Regel limit. These findings underscore the intricate relationship between interlayer twisting and phonon thermal transport in penta-$PdTe_2$, providing new insights into the thermal transport and phonon engineering in the 2D pentagonal family of materials.

Supporting Information

Supporting Information is available from the Wiley Online Library or from the author.

Acknowledgements

This work was partially supported by a grant from the National Natural Science Foundation of China (Grant No. NSFC-12274007) and was also supported by the High-Performance Computing Platform of Peking University, China. P. J. acknowledges partial support by the U.S. Department of Energy, Office of Basic Energy Sciences, Division of Materials Sciences and Engineering under award DE-FG02-96ER45579.

Conflict of Interest

The authors declare no conflict of interest.

Data Availability Statement

The data that support the findings of this study are available from the corresponding author upon reasonable request.

Keywords

lattice thermal conductivity, penta-sheet, twisting, universal machine-learning potential, Wigner transport

Received: August 12, 2025
Revised: November 24, 2025
Published online: December 12, 2025

[1] S. Carr, S. Fang, E. Kaxiras, *Nat. Rev. Mater.* **2020**, *5*, 748.
[2] X. Sun, M. Suriyage, A. R. Khan, M. Gao, J. Zhao, B. Liu, M. M. Hasan, S. Rahman, R.-S. Chen, P. K. Lam, *Chem. Rev.* **2024**, *124*, 1992.
[3] Y. Chen, C. Zhang, J. Sun, D. Ni, C. Zhang, Q. Wang, *Appl. Surf. Sci.* **2023**, *635*, 157718.
[4] J. Sun, M. Hu, C. Zhang, L. Bai, C. Zhang, Q. Wang, *Adv. Funct. Mater.* **2022**, *32*, 2209000.
[5] C. Zhang, J. Sun, Y. Shen, C. Zhang, Q. Wang, A. Yoshikawa, Y. Kawazoe, P. Jena, *Small* **2023**, *19*, 2303295.
[6] C. Zhang, Y. Chen, Q. Wang, P. Jena, *Nano Lett.* **2025**, *25*, 8689.
[7] Y. Shen, Q. Wang, *Phys. Rep.* **2022**, *964*, 1.
[8] C. Zhang, J. Sun, Y. Shen, W. Kang, Q. Wang, *J. Phys. Chem. Lett.* **2022**, *13*, 5734.
[9] L. Liu, Y. Ji, M. Bianchi, S. M. Hus, Z. Li, R. Balog, J. A. Miwa, P. Hofmann, A.-P. Li, D. Y. Zemlyanov, *Nat. Mater.* **2024**, *23*, 1339.
[10] Y. Qu, C. T. Kwok, Y. Shao, X. Shi, Y. Kawazoe, H. Pan, *Int. J. Hydrogen Energy* **2021**, *46*, 9371.
[11] P. Sharma, V. Roondhe, A. Shukla, *Phys. Rev. B* **2024**, *110*, 214108.
[12] C. Hou, J. Xin, Y. Shen, Y. Guo, Q. Wang, *J. Phys. Chem. Lett.* **2025**, *16*, 7177.
[13] Y.-S. Lan, X.-R. Chen, C.-E. Hu, Y. Cheng, Q.-F. Chen, *J. Mater. Chem. A* **2019**, *7*, 11134.
[14] L. Li, Z. Huang, J. Xu, H. Huang, *Front. Chem.* **2022**, *10*, 1061703.
[15] M. Omini, A. Sparavigna, *Physica B: Condens. Matter* **1995**, *212*, 101.
[16] D. A. Broido, M. Malorny, G. Birner, N. Mingo, D. Stewart, *Appl. Phys. Lett.* **2007**, *91*, 231922.
[17] T. Feng, X. Ruan, *Phys. Rev. B* **2016**, *93*, 045202.
[18] M. Simoncelli, N. Marzari, F. Mauri, *Nat. Phys.* **2019**, *15*, 809.
[19] M. Simoncelli, N. Marzari, F. Mauri, *Phys. Rev. X* **2022**, *12*, 041011.
[20] A. V. Shapeev, *Multiscale Model. Simul.* **2016**, *14*, 1153.
[21] Z. Fan, Z. Zeng, C. Zhang, Y. Wang, K. Song, H. Dong, Y. Chen, T. Ala-Nissila, *Phys. Rev. B* **2021**, *104*, 104309.
[22] Z. Fan, *J. Phys.: Condens. Matter* **2022**, *34*, 125902.
[23] T. Liang, K. Xu, E. Lindgren, Z. Chen, R. Zhao, J. Liu, E. Berger, B. Tang, B. Zhang, Y. Wang, arXiv **2025**, arXiv:2504.21286.
[24] P. Lazić, *Comput. Phys. Commun.* **2015**, *197*, 324.
[25] Z. Fan, H. Dong, A. Harju, T. Ala-Nissila, *Phys. Rev. B* **2019**, *99*, 064308.
[26] Z. Fan, Y. Wang, P. Ying, K. Song, J. Wang, Y. Wang, Z. Zeng, K. Xu, E. Lindgren, J. M. Rahm, *J. Chem. Phys.* **2022**, *157*, 114801.
[27] P. E. Blöchl, *Phys. Rev. B* **1994**, *50*, 17953.
[28] G. Kresse, D. Joubert, *Phys. Rev. B* **1999**, *59*, 1758.
[29] G. Kresse, J. Furthmüller, *Phys. Rev. B* **1996**, *54*, 11169.
[30] J. P. Perdew, K. Burke, M. Ernzerhof, *Phys. Rev. Lett.* **1996**, *77*, 3865.
[31] Y. Hu, C. Storey, *J. Optim. Theory. Appl.* **1991**, *69*, 139.
[32] J. Klimeš, D. R. Bowler, A. Michaelides, *J. Phys.: Condens. Matter* **2009**, *22*, 022201.
[33] E. Bitzek, P. Koskinen, F. Gähler, M. Moseler, P. Gumbsch, *Phys. Rev. Lett.* **2006**, *97*, 170201.
[34] J. Larkin, J. Turney, A. Massicotte, C. Amon, A. McGaughey, *J. Comput. Theor. Nanosci.* **2014**, *11*, 249.
[35] A. Carreras, A. Togo, I. Tanaka, *Comput. Phys. Commun.* **2017**, *221*, 221.
[36] A. P. Thompson, H. M. Aktulga, R. Berger, D. S. Bolintineanu, W. M. Brown, P. S. Crozier, P. J. In't Veld, A. Kohlmeyer, S. G. Moore, T. D. Nguyen, *Comput. Phys. Commun.* **2022**, *271*, 108171.
[37] Z. Sun, K. Yuan, X. Zhang, G. Qin, X. Gong, D. Tang, *Phys. Chem. Chem. Phys.* **2019**, *21*, 15647.
[38] A. D. Oyedele, S. Yang, L. Liang, A. A. Puretzky, K. Wang, J. Zhang, P. Yu, P. R. Pudasaini, A. W. Ghosh, Z. Liu, *J. Am. Chem. Soc.* **2017**, *139*, 14090.
[39] L. Chen, W. Zhang, H. Zhang, J. Chen, C. Tan, S. Yin, G. Li, Y. Zhang, P. Gong, L. Li, *Sustainability* **2021**, *13*, 4155.
[40] M. K. Gupta, S. Kumar, R. Mittal, S. K. Mishra, S. Rols, O. Delaire, A. Thamizhavel, P. Sastry, S. L. Chaplot, *J. Mater. Chem. A* **2023**, *11*, 21864.
[41] Q. Ren, M. K. Gupta, M. Jin, J. Ding, J. Wu, Z. Chen, S. Lin, O. Fabelo, J. A. Rodríguez-Velamazán, M. Kofu, *Nat. Mater.* **2023**, *22*, 999.
[42] H. Zhou, J. Tiwari, T. Feng, *Phys. Rev. Mater.* **2024**, *8*, 043804.
[43] A. Ioffe, A. Regel, *Prog. Semicond.* **1960**, *4*, 237.

[44] W. Keune, S. Hong, M. Y. Hu, J. Zhao, T. Toellner, E. E. Alp, W. Sturhahn, T. Rahman, B. R. Cuenya, *Phys. Rev. B* **2018**, *98*, 024308.
[45] L. Yang, N. Yang, B. Li, *Sci. Rep.* **2013**, *3*, 1143.
[46] R. Milkus, A. Zaccone, *Phys. Rev. B* **2016**, *93*, 094204.
[47] A. Giri, B. F. Donovan, P. E. Hopkins, *Phys. Rev. Mater.* **2018**, *2*, 056002.
[48] M. Samanta, K. Pal, P. Pal, U. V. Waghmare, K. Biswas, *J. Am. Chem. Soc.* **2018**, *140*, 5866.